Disconnecting symmetry breaking from seeded growth for the reproducible synthesis of high quality gold nanorods

Disconnecting Symmetry Breaking From Seeded Growth for Reproducible Synthesis of High Quality Gold Nanorod

Guillermo González-Rubio[†‡], Vished Kumar[†], Pablo Llombart [§ ‡], Pablo Díaz-Núñez[⊥], Eva Bladt[‖], Thomas Altantzis [‖], Sara Bals [‖], Ovidio Peña-Rodríguez [⊥], Eva G. Noya[§], Luis G. MacDowell[‡], Andrés Guerrero-Martínez*[‡], Luis M. Liz-Marzán*[†#]*

[†]CIC biomaGUNE and CIBER-BBN, Paseo de Miramón 182, 20014 Donostia–San Sebastián, Spain.

[‡]Departamento de Química Física, Universidad Complutense de Madrid, Avenida Complutense s/n, 28040 Madrid, Spain.

[§] Instituto de Química Física Rocasolano, CSIC, Calle Serrano 119, E-28006 Madrid, Spain

[⊥]Instituto de Fusión Nuclear, Universidad Politécnica de Madrid, José Gutiérrez Abascal 2, E-28006 Madrid, Spain.

[‖]EMAT-University of Antwerp, Groenenborgerlaan 171, B-2020 Antwerp, Belgium

[#]Ikerbasque (Basque Foundation for Science), 48013 Bilbao, Spain.

*Corresponding authors. Email: ggrubio@ucm.es (G.G.-R.), aguerrero@quim.ucm.es (A.G.-M.), llizmarzan@cicbiomagune.es (L.M.L.-M.)

ABSTRACT

One of the major difficulties hindering the widespread application of colloidal anisotropic plasmonic nanoparticles is the limited robustness and reproducibility of multistep synthetic methods. We demonstrate herein that the reproducibility and reliability of colloidal gold nanorod synthesis can be greatly improved by disconnecting the symmetry breaking event from the seeded growth process. We have used a modified silver-assisted seeded growth method in the presence of hexadecyltrimethylammonium bromide (CTAB) and *n*-decanol as the co-surfactant to prepare small gold nanorods in high yield, which were then used as seeds for the growth of high quality Au nanorod colloids. Whereas the use of *n*-decanol provides a more rigid micellar system, the growth on anisotropic seeds avoids sources of irreproducibility during the symmetry breaking step, yielding uniform nanorod colloids with narrow plasmon bands, ranging from 600 to 1250 nm, and allowing fine tuning of the final dimensions. This method provides a robust route for the preparation of highly-quality gold nanorod colloids with tunable morphology, size and optical response, in a reproducible and scalable manner.

KEYWORDS: gold nanorods, CTAB, *n*-decanol, symmetry breaking, seeded growth

Noble metal nanocrystals have become an essential component for the development of improved technologies for biomedicine,[1] energy harvesting,[2] or chemical synthesis,[2] among others.[3,4] Importantly, the overall usefulness and potential relevance of metal nanocrystals relies on our capacity to control their shape and, hence, their optical properties. Although the nature, purity, and concentration of chemical reactants are pivotal toward obtaining the desired metal nanocrystals, the uniformity in shape and size of the final metal nanoparticles relies ultimately on the employed methodology.[5,6]

The advent of colloidal seed-mediated growth methods in the early 2000's entailed a breakthrough in the synthesis of noble metal nanoparticles.[7,8] Based on the spatial and temporal separation between nanocrystal nucleation and growth, this methodology provided access to colloidal metal nanocrystals[9] in a wide variety of shapes, including spheres,[10] rods,[11] or triangles.[12] Moreover, seeded growth has proven to be the most efficient method toward gaining insight into the growth mechanisms of anisotropic nanocrystals.[13–15] The concept was first introduced by Murphy *et al.* for the synthesis of gold nanorods (AuNRs),[7] which is probably the most alluring case of anisotropic noble metals synthesis. Due to the high-symmetry face-centered cubic lattice of gold (as well as of other noble metals), its growth into low-symmetry nanocrystals is highly unfavored.[5] Nonetheless, the silver-assisted seeded growth of AuNRs demonstrated that anisotropic nanoparticles can be prepared in shape yields over 99%.[16–18] Not surprisingly, the underlying mechanism responsible for AuNR formation has been the focus of intense research during the last decade.

Nevertheless, the complexity of the mixture of surfactant and salts where AuNR growth takes place, makes it difficult to unravel the underlying mechanisms and to achieve the desired reproducibility. For instance, the role of the surfactant hexadecyltrimethylammonium bromide (CTAB, required for the synthesis of AuNRs), has been claimed to be related to the

induction of strain, favoring anisotropic growth, and the modification of the electrochemical potential of gold ions.[19,20] Additionally, when single crystal seeds are used, the presence of silver ions in solution is required for symmetry breaking to occur.[11,15–18] In addition, a certain degree of truncation should be allowed in the seed to initiate anisotropic growth, thereby restricting the seeds size to the range between 4 - 7 nm. In this regard, the aspect ratio is determined by the $[HAuCl_4]/[AgNO_3]$ ratio, symmetry breaking occurring at the smaller seed sizes for high silver concentration, thereby producing AuNRs of higher aspect ratio.[13–15] Finally, solution pH, temperature, and concentration of ascorbic acid (weak reducing agent) also influence the outcome of AuNR growth. Therefore, symmetry breaking occurs only within a narrow range of reactant concentrations, seed sizes, and experimental conditions. As a result, the lack of reproducibility remains the main drawback of the currently used methods for AuNR growth.[21]

In this work, we explored a different concept toward a reproducible and reliable method for the silver-assisted seed-mediated synthesis of AuNRs. As such, we envisioned that control over the formation of AuNRs can be achieved by optimizing separately the symmetry breaking and seeded growth stages. This concept requires the preparation of intermediate anisotropic seeds (small AuNRs), which then serve as universal seeds for the growth of AuNRs with selected aspect ratio and size. This approach thus becomes much more robust and scalable than current methods, so that the plasmonic properties and dimensions of the obtained AuNRs can be readily tuned with high simplicity and reproducibility. Furthermore, we introduce the use of *n*-decanol as a co-surfactant that can enter CTAB micellar aggregates, as an important additive for optimization of the symmetry breaking step and the overall success of the method. Computational studies on the interactions between surfactant aggregates and different gold facets, support a model that allowed us to understand the underlying mechanism of *n*-decanol action.

RESULTS AND DISCUSSION

It has been established that, besides the experimental conditions, the shape, size, and crystal habit of the seeds determine the quality of the products resulting from the seed-mediated growth of metal nanoparticles.[9,15,22–24] In the particular case of AuNR synthesis, the efficiency of the symmetry breaking process is highly sensitive to small variations in the 1–2 nm nanocrystalline seed.[21,25] However, the reproducible synthesis of 1–2 nm seeds of sufficient quality remains a challenge. Furthermore, the small seeds are only stable for a few hours (due to Ostwald ripening processes) and freshly prepared seed solutions are required whenever a new batch of AuNRs is prepared.[26] In this context, the main idea behind our work is that the reproducibility of the seed-mediated silver-assisted synthesis of AuNRs could be significantly improved by optimizing the symmetry breaking process in a step that is separated from anisotropic growth, both in space and time. Accordingly, the preparation of stable anisotropic gold seeds (where the symmetry breaking process has been completed) should allow us to improve the reproducibility of current methods for AuNR synthesis. In practice, this involves the synthesis of small gold nanorods in high yield and their subsequent use as small anisotropic seeds to obtain AuNRs of different aspect ratios and/or dimensions (**Figure 1**).

-

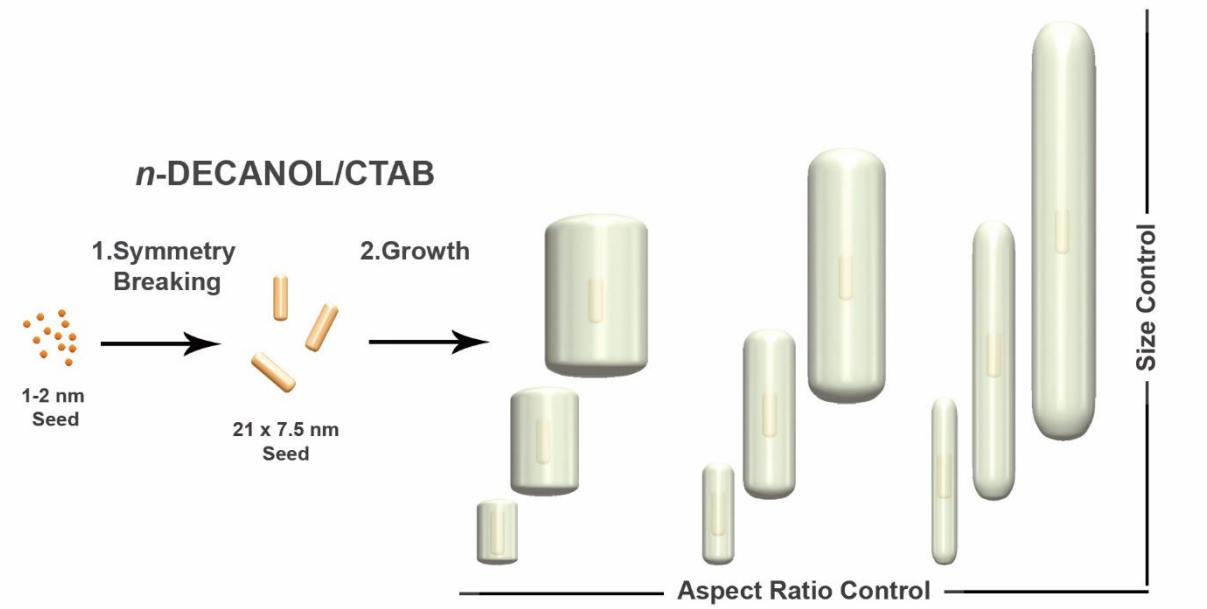

Figure 1. Schematics of the proposed method for the reproducible synthesis of AuNRs. Small 1-2 nm gold seeds are used to prepare anisotropic 21 × 7.5 nm gold nanocrystals, where symmetry breaking (1) has been completed, The anisotropic seeds are then used for the controlled growth (2) of colloidal AuNRs with low dispersity in both aspect ratio and size.

Although both seed-mediated and seedless approaches have been developed for the synthesis of anisotropic nanocrystals of reduced dimensions (volume *ca.* 10^3 nm^3), their preparation in high yield has remained elusive.[27–29] Several issues are encountered, most of them related to the shape yield (usually below 90%) and overall size dispersity. Still, reproducibility remains the main obstacle toward the synthesis of small anisotropic nanocrystals with low size dispersity. Aromatic molecules (*e.g.* bromo salicylic acid)[16,18] and oleic acid[17] have been introduced as additives to modify the nature of micellar CTAB aggregates, thereby significantly improving the preparation of standard AuNRs in high yield (99%). Therefore, we propose that the use of an additive can cooperate with CTAB in favoring the preparation of small anisotropic nanocrystals in high yield. However, such additives present a concomitant co-reducing role that makes the analysis of their colloidal effects on the

synthesis process difficult. As an alternative, long linear-chain alcohols such as *n*-decanol, can be solubilized within CTAB micelles as co-surfactants, stimulating their growth and leading to structural transitions from spherical to worm-like micelles and lamellar structures.[31] For this reason, we decided to investigate the use of *n*-decanol in the synthesis of small anisotropic nanocrystals, affording (i) high shape yield, (ii) controlled dimensions, and (iii) improved reproducibility (**Figure 2**).

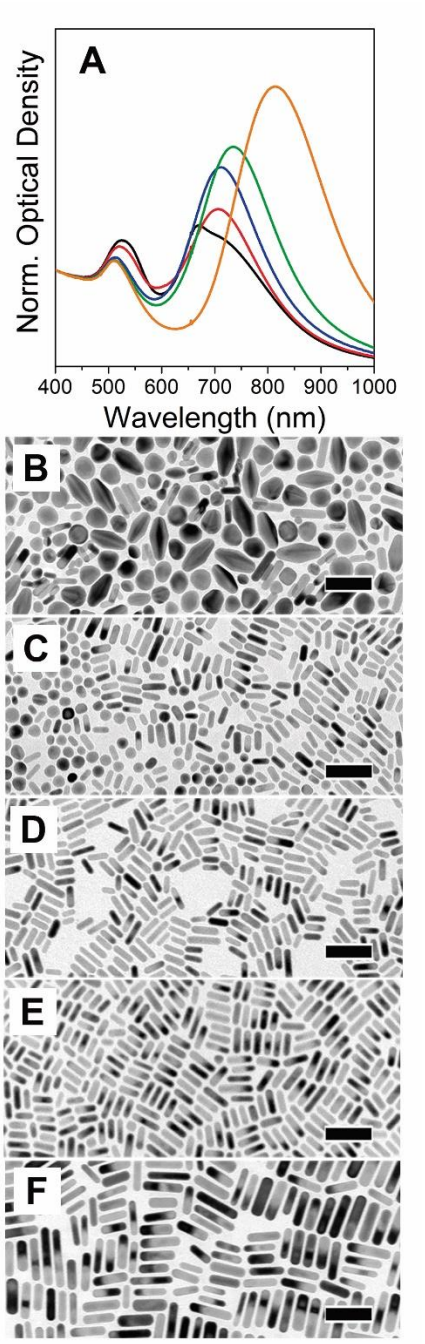

Figure 2. Synthesis of small anisotropic seeds. (A) Normalized optical density spectra and (B–F) representative TEM images of small AuNRs obtained at different *n*-decanol/CTAB ratios: 0.23 (black, B), 0.25 (red, C), 0.27 (blue, D), 0.29 (green, E), and 0.31 (magenta, F). Scale bars: 50 nm.

The synthesis of small AuNRs was carried out following the standard method with some modifications (see Methods Section and Supporting Information for details) but introducing *n*-decanol in different *n*-decanol/CTAB ratios between 0.23 and 0.31 for optimization. The UV-Vis spectral analysis of the products showed the presence of two distinct extinction bands, suggesting the formation of AuNRs (for which the bands can be assigned to transversal and longitudinal LSPR modes). The longitudinal LSPR band became more intense and gradually red-shifted (from 710 to 750 nm) with increasing *n*-decanol content (**Figure 2A**). Analysis of TEM images revealed that small anisotropic seeds were successfully produced, only at *n*-decanol/CTAB ratios between 0.27 and 0.29 (yield = 98%; length = 20±3.5 nm, width = 7.5±1.5 nm, volume: (0.9 ±0.2)× 10^3 nm^3, **Figures 2B–F**, **S1, S2**). Below the optimal *n*-decanol/CTAB ratio, the products mostly contained large spheres and short bipyramids (**Figure 2B**) or a mixture of small anisotropic and spherical nanocrystals (**Figure 2C**). At the highest studied *n*-decanol content, they were also produced in high yield, but their dimensions were significantly larger (length = 36±9 nm, width = 10±1.5 nm, **Figure 2F**). In the absence of *n*-decanol, small anisotropic seeds can also be obtained after the growth conditions have been re-optimized. However, the dispersion in size and shape are much wider (**Figure S3**).

We hypothesized that the role of *n*-decanol would be related to the selective passivation and stabilization of certain facets in the seeds, by CTAB aggregates during the symmetry breaking event. It has been demonstrated that seeded growth of single crystal gold nanorods requires the use of cuboctahedral seeds, *i.e.* gold nanocrystals enclosed by six {001} and eight {111} facets. As the size of the seed increases, truncating {110} facets may stochastically appear as a way to remove high-energy edge atoms located at intersections between {111} facets. For small nanocrystals (4-6 nm) this could lead to truncating surfaces appearing only at certain intersections between {111} facets and the rupture of the

nanocrystal symmetry. [13–15] Then, the presence of silver ions could render preferential stabilization of newly formed {110} facets over the {001} and {111} ones, *via* an underpotential deposition mechanism and the growth of the nascent AuNRs develops orthogonally on the new facets (along the ⟨100⟩ direction) [14,31] In addition to silver ions, CTAB has also been proposed to play a key role in the stabilization of emerging facets.[32,33] As such, CTAB remains the most employed surfactant for the synthesis of AuNRs. The hypothesis is that CTAB colloidal aggregates adsorb strongly on high-index facets, reducing the accessibility for gold ions. Therefore, modification of the CTAB aggregation behavior by insertion of *n*-decanol molecules should affect the passivation of truncating surfaces, possibly explaining the observed increased efficiency in the symmetry breaking process and synthesis of small AuNRs.

To validate this hypothesis, we confirmed the insertion of *n*-decanol in CTAB aggregates by means of diffusion-ordered NMR spectroscopy (DOSY) (**Figure S4**).[34] The analysis of DOSY spectra upon addition of *n*-decanol to small gold nanorods stabilized with CTAB under experimental conditions of synthesis (see Methods Section), showed: (i) a significant decrease in the self-diffusion coefficient of CTAB (from 6.7×10^{-11} m^2 s^{-1} to 2.9×10^{-11} m^2 s^{-1}), and (ii) the same self-diffusion coefficients for *n*-decanol and CTAB when mixed in solution. Additionally, we found no changes in the self-diffusion coefficient of water (1.98×10^{-9} m^2 s^{-1}), which confirms that there are no significant changes in the global viscosity of the solutions.[34] Interestingly, negligible modifications of the self-diffusion coefficient of CTAB were observed upon addition of *n*-decanol in the absence of gold nanorods (Figure S4A, B). Therefore, all these results point to an increase in the effective size of CTAB aggregates adsorbed onto gold nanorods, due to the formation of mixed *n*-decanol/CTAB micelles.

Then, we carried out a series of Molecular Dynamics (MD) simulations of the aggregation behavior of *n*-decanol/CTAB mixtures on different gold surfaces using the GROMACS Package (**Figure S5**, **Table S1**).[35] Whereas it has been reported that CTAB bilayers in solution are unstable and small spherical micelles are preferred,[6] *n*-decanol/CTAB solutions form stable bilayers at ratios between 0.20–0.30, in good agreement with the concentrations at which we experimentally found better results in the formation of AuNRs. Lower and higher *n*-decanol contents destabilize the bilayer in favor of micellar aggregates. Preassembled CTAB bilayers,[36] with varying concentrations of *n*-decanol, are initially deposited on {001}, {111}, and {110} gold surfaces, which are expected to form during the early stages of AuNR growth.[14] Higher-index facets such as {250} were also studied regarding their emergence at increasing AuNR dimensions.[37,38] The system was then solvated with $AuCl_2^-$ anions acting as the gold source and H_3O^+ cations to maintain the neutrality of the system. The simulations revealed highly surface-specific interactions of gold with the *n*-decanol/CTAB aggregates, resulting in different self-assembled morphologies, affecting the diffusion of gold ions from the bulk solution toward the AuNR surface. On {110} and {250} facets, pre-assembled bilayers remain highly ordered and homogeneously cover the gold surface; on the {100} and {111} surfaces, however, the bilayer gets destabilized and tends to form micellar aggregates with a heterogeneous coverage. The structure of *n*-decanol/CTAB aggregates was found to have a large impact on the ability of gold ions to diffuse toward the particle surface. When CTAB forms micelles, *e.g.* on {100} and {111}-type facets, gold ions can readily access the gold surface from solution by diffusion on the micelle surface (**Figure 3A**). On the contrary, when a rigid bilayer is formed on the particle surface, gold ions would be required to cross such a *n*-decanol/CTAB bilayer to reach the gold surface, but this effect was not observed in the timescale of our simulations. Instead, gold ions diffused along the surface of the bilayer, still exposed to the solution (**Figure 3B**). We quantified these different

behaviors by measuring the separation distance of gold ions to the surface (**Figure 3C**). We found that, whereas gold ions were able to reach the gold surface in the presence of micelles, they fluctuated and moved along the bilayer interface when more compact aggregates were present. Upon close observation, one can see that gold ions can also penetrate the aggregates in this instance, but they are swiftly expelled out again. We additionally calculated the probability of finding gold ions at a threshold distance of 1 nm from the surface (**Figure 3D**). The availability of gold ions exhibits a maximum for {100} facets at *n*-decanol/CTAB ratios between 0.20 and 0.30, in agreement with the concentrations at which the experiments showed growth of more uniform small AuNRs. The availability of gold ions on the {111} surfaces is also significant for *n*-decanol/CTAB ratios in the range of 0.10–0.30, though much lower than on {100} surfaces. On the contrary, the availability of gold ions on {110} and {250} facets is very low for all the studied *n*-decanol percentages. Computer simulations thus support a significant influence of *n*-decanol to enhance the selective CTAB passivation of high-index facets. Since the presence of silver ions is pivotal for the symmetry breaking event to occur, we also studied the role of *n*-decanol/CTAB aggregates in the avaibility of silver ions on different gold facets (Figure S6). We found that diffusion of silver ions through the *n*-decanol/CTAB aggregates is not favored and the differences between different facets are negligible. This result might indicate that the effect of *n*-decanol is mainly related to changes in the diffusion of gold ions, but hardly affecting Ag^+ diffusion. Therefore, in the presence of *n*-decanol (and silver ions), symmetry breaking in the crystalline gold seed is more efficient and thus small anisotropic seeds are systematically obtained in high yield.

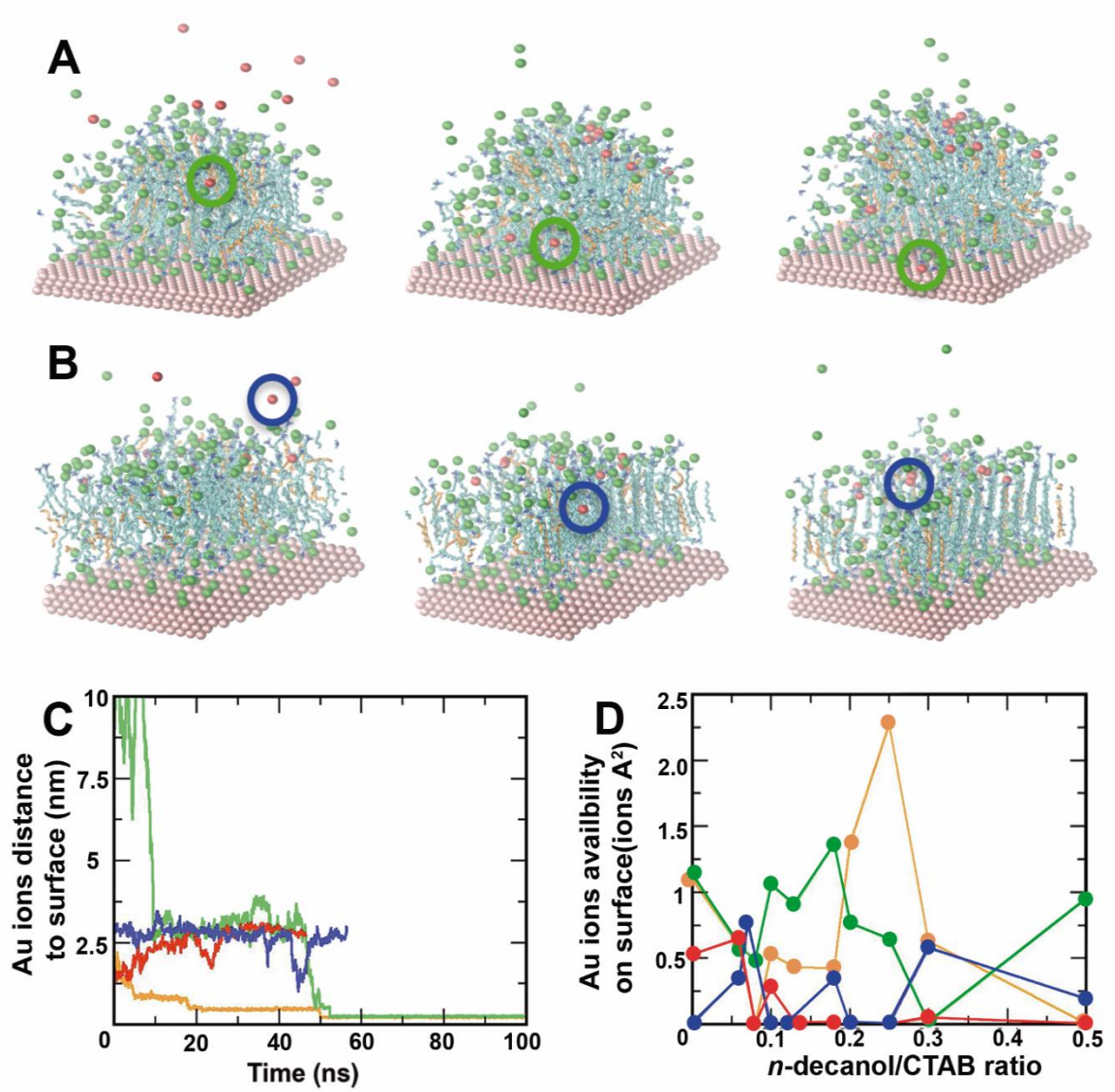

Figure 3. Role of *n*-decanol in the synthesis of small anisotropic seeds. (A,B) Mechanism of diffusion of $AuCl_2^-$ anions in the presence of *n*-decanol/CTAB aggregates (green and blue lines depict the trajectory of gold ions at different times of the simulation). (A) On {111} surfaces, the micelles cover the surface heterogeneously and the diffusion of gold ions toward the gold surface is facilitated. (B) On {250} surfaces, the surfactants form bilayers with homogeneous coverage, hindering the diffusion of gold ions toward the surface. Gold ions are shown as red spheres, bromide ions as green spheres, surfactant chains as blue lines, *n*-decanol in orange, and gold surfaces in pink. (C) Distance of gold ions to the gold surface for selected trajectories: orange ({100} facets) and green ({111} facets) lines show the trajectories corresponding to the mechanism in (A), while red ({110} facets) and blue ({250} facets) lines show the typical diffusion expected for the mechanism shown in (B). (D)

Probability of finding gold ions at a distance smaller than 1 nm from the gold surface for the different facets: {100} (orange), {111} (green), {110} (red), and {250} (blue).

Once the fabrication of small anisotropic seeds was successfully optimized by the addition of *n*-decanol, we focused on the seeded growth of high-quality AuNR colloids. Even though the concept of growth on pre-formed AuNRs has been widely reported in the literature,[39–41] the tunability of longitudinal LSPR frequency that can be achieved by this method is rather limited. Similarly, when larger anisotropic seeds are used, the growth homogeneity is again reduced, resulting in asymmetric and/or broad LSPR bands (**Figure 4A**, **Figures S7–S11**, **Table S2**). Collectively, these pieces of evidence suggest that the use of AuNRs with reduced dimensions is central toward the synthesis of high-quality AuNR colloids with widely tunable LSPR bands. We hypothesized that high-index facets form at the tips of AuNRs as their dimensions increase, which are subsequently stabilized by deposition of silver and surfactant micelles.[14,41] While we expect the sides of AuNRs at early stages of growth (*i.e.* small AuNRs) to be enclosed by {001} and {111} facets, truncating surfaces appear at more advanced stages thereby suppressing edges between existing facets. Anisotropic growth is favored when such surfaces are exclusively located at the sides. However, as AuNRs keep growing, the formation of high-index facets may also develop at the tips. Silver and surfactant aggregates thus stabilize both the tips and sides, so that gold deposition is no longer preferential at the tips. As a consequence, anisotropic growth is enhanced in small AuNRs due to the lower proportion of high-index facets expected at the tips.

Considering the effect of *n*-decanol in small anisotropic seeds formation, the additive was also used in the homogeneous seeded growth on the AuNRs (**Figure 4B,C**). At *n*-decanol/CTAB ratios around 0.22, the intensity of the LSPR bands was consistently highest,

regardless of the growth conditions. Importantly, the amount of $HAuCl_4$ was fixed in all experiments, whereas the amounts of $AgNO_3$ and HCl (pH), as well as temperature were varied. In summary, we carried out experiments at three different temperatures: 18 °C, 28 °C, and 38 °C; two $[HAuCl_4]/[AgNO_3]$ ratios: 3.3 and 1.7; and two $[HCl]/[HAuCl_4]$ ratios: 60 and 120 (**Figure 4B,C**, **Figures S12–S14**, **Table S3**). The aspect ratio dispersity (*D*, defined as the standard deviation from the mean value, expressed in percentage) was calculated by means of optical fits to the LSPR bands of AuNRs prepared at different *n*-decanol concentrations (see Supporting Information for details; **Figures S12-S14**).[6,43,44] This method is more reliable than the usual analysis based on TEM images (see also **Figures S12–S14**, **Table S3**), where a much smaller number of particles are actually analyzed (few hundreds versus ca. 10^{11}), distortions may be introduced during TEM sample preparation, and low image quality (poor image resolution and/or low contrast) may lead to errors in the analysis.[6,43] The lowest aspect ratio dispersity (6.25–7%) was obtained at *n*-decanol/CTAB ratios ranging from 0.20 to 0.24. In contrast, pure CTAB (*D* = 9.5% at all three temperatures) and 0.30 *n*-decanol/CTAB (*D* = 11–12.5%) afforded less homogeneous growth.

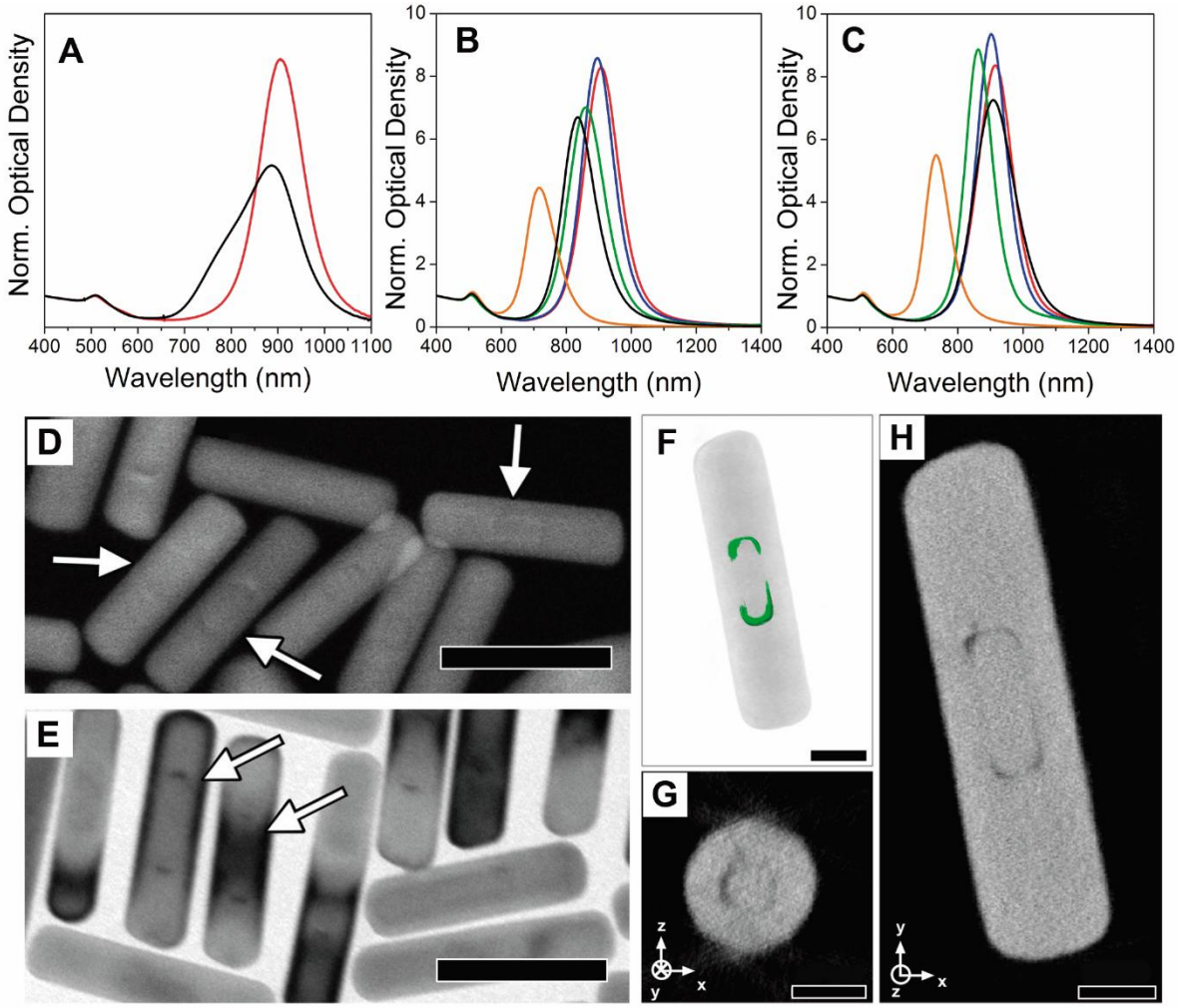

Figure 4. Effect of small anisotropic seeds dimensions and *n*-decanol proportion on the growth process, and their location inside the final AuNRs. (A) Normalized optical density spectra of AuNRs obtained by seeded growth on small anisotropic seeds (length: 21 nm, width: 7.5 nm, red) and on anisotropic seeds of similar aspect ratio but larger size (length: 36 nm, width: 10.5 nm, black). (B,C) Normalized optical density spectra of small AuNRs prepared in the presence of increasing *n*-decanol/CTAB ratios: 0 (pure CTAB, black), 0.20 (red), 0.22 (blue), 0.24 (green), and 0.30 (orange), under different experimental conditions: (B) $[HAuCl_4]/[AgNO_3]$ = 3.3 and $[HCl]/[HAuCl_4]$ = 60 at 18 °C; (C) $[HAuCl_4]/[AgNO_3]$ = 1.7 and $[HCl]/[HAuCl_4]$ = 120 at 28 °C. (D) Low magnification HAADF-STEM and (E) TEM images of AuNRs prepared by seeded growth on small anisotropic seeds coated with a thin shell of Pd. The white arrows indicate the position of the Au@Pd seeds inside the final AuNRs. Scale bars: 50 nm. (F) 3D visualization of the reconstructed volume of an individual AuNR, where the Au@Pd seed is indicated in green (manual segmentation). Scale bar: 10 nm. (G,H) Orthoslices in the *xz* (G) and *xy* (H) planes through the reconstruction, showing a

lower intensity at the Pd location (Pd has a lower atomic number than Au). Scale bars: 10 nm.

An interesting advantage of this method is that it allows the visualization of the small anisotropic seed inside the final AuNR. For this purpose, a thin layer of palladium was grown on the small anisotropic seeds (Au@Pd seeds, see Methods Section), prior to seeded growth.[22,45] Because of the lower atomic number of palladium relative to that of gold (Z_{Pd} = 46 and Z_{Au} = 79), the position of the small Au@Pd seeds could be observed in high angle annular dark field scanning transmission electron microscopy (HAADF-STEM) mode, since the intensity in such images scales with the projected thickness of the structure and the atomic number of the elements (**Figure 4D–H**).[22] By using high angle annular dark field STEM (HAADF-STEM) tomography, we were able to determine that the deposition of Pd atoms occurs preferentially at the tips of the AuNR seeds (**Figure 4F–H**). More importantly, the HAADF-STEM images show that anisotropic growth is clearly imposed by the geometry of the small Au@Pd seeds, which is located around the geometrical center of the grown AuNR (Figure 4F–H).

Beyond the narrower LSPRs bands obtained (**Figure S15-S18**) during optimization of the CTAB/*n*-decanol system (compared to standard two-steps methods, where symmetry breaking event is not disconnected form the growth process), we identified the most appealing feature of this method: the straightforward tunability of the longitudinal LSPR. For instance, by simply increasing the [HCl]/[$HAuCl_4$] ratio from 40 to 160, the LSPR band was readily shifted from 760 to 1125 nm, barely affecting the AuNR size and shape dispersity (*D* < 10%, **Figure 5A**, **Figures S15-S22** , **Table S4** and **S5**). This effect can be related to a lower redox potential of ascorbic acid at low pH, which results in a slower growth kinetics and favored anisotropic growth.[14] On the contrary, when the growth was seeded on 1–2 nm gold nanocrystals (the standard two-step method), only [HCl]/[$HAuCl_4$] ratios in a narrow range

(60–80) lead to high yields of high-quality AuNRs (**Figure 5B**, **Figure S17**). In this case, the LSPR can also be tuned within a similar range, above the optimum HCl amount, but at the expense of increasing the population of spherical impurities, as indicated by a shoulder at 525–535 nm and seen in TEM images (**Figures S19–S22**). We further note that, the overall size of the overgrown AuNRs could be better adjusted when the symmetry breaking is disconnected from the growth (**Figure 5C–H**, **Tables S4 and S5**).

We also compared the growth of AuNRs using either small anisotropic nanocrystals or 1–2 nm spherical nanocrystals as seeds, both at the same $[HAuCl_4]/[AgNO_3]$ ratio of 3.3. The optimal growth temperature was different in both cases. For instance, the use of 1–2 nm gold seeds required a temperature of 28 °C to afford the highest AuNR yield. Interestingly, narrower LSPR bands were obtained when using small AuNRs at 16 °C instead of 28 °C (**Figure S23**). This fact suggests that, for the studied $[HAuCl_4]/[AgNO_3]$ ratios, symmetry breaking and subsequent growth may be favored at 28 °C, but narrower bands (higher size and aspect ratio dispersity) can be obtained when anisotropic growth is disconnected from symmetry breaking and performed at 16 °C. Similar results were obtained for other $[HAuCl_4]/[AgNO_3]$ ratios (**Figure S23**).

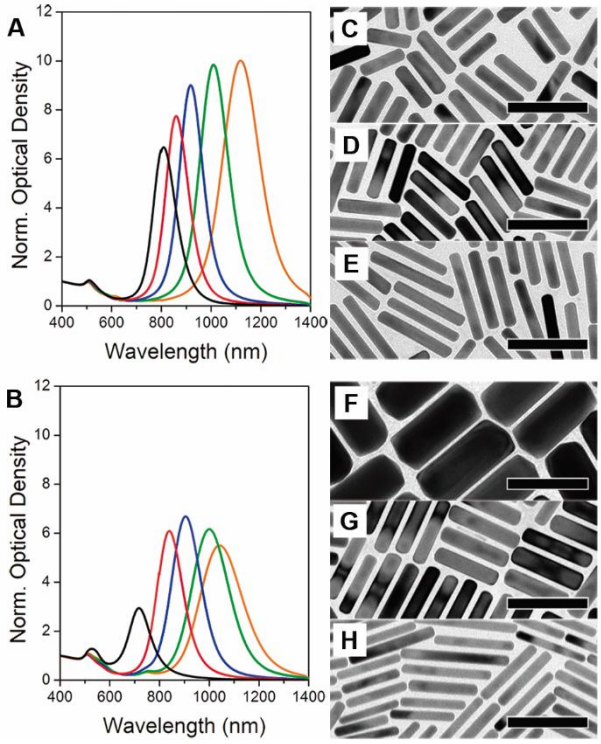

Figure 5. Comparison between the use of small anisotropic seeds and standard Au nanocrystal seeds in the growth of AuNRs at increasing [HCl]/[$HAuCl_4$] ratios. (A,B) Normalized optical density spectra of AuNRs obtained *via* seeded growth on either small AuNRs (A) or 1–2 nm Au nanocrystals (B), at [HCl]/[$HAuCl_4$] ratios of 40 (black), 60 (red), 80 (blue), 120 (green), and 160 (orange). (C–H) TEM images of AuNRs synthesized at [HCl]/[$HAuCl_4$] ratios of 40, 80, and 160 by seeded growth on either 21 × 7.5 nm anisotropic seeds (C–E) or 1–2 nm Au nanocrystals (F–H), respectively. Scale bars: 100 nm.

To explain how silver ions enable control over AuNR growth, a mechanism based on underpotential deposition (UPD) on lateral, high-index facets has been proposed.[14,31] The deposition of silver ions *via* UPD in the presence of excess gold ions during the growth process favors the formation of a self-sustaining cycle of silver co-reduction and galvanic replacement by gold ions. This process is affected by temperature, which is in agreement with the above described dependence of the optimal [$HAuCl_4$]/[$AgNO_3$] ratio with temperature.

Indeed, we found that at 16 °C the optimal $[HAuCl_4]/[AgNO_3]$ ratio ranged from 2.5 to 3.3, whereas ratios higher than 3.3 were required at 28 ºC and 38 °C (**Figure S23**).

By controlling pH, temperature, Ag^+ concentration and reducing agent, AuNRs with LSPR bands ranging from 600 up to 1270 nm could be successfully grown with high-quality (**Figure 6A–F, Figure S24, S25, Tables S6 and S7**). Our methodology yields AuNRs featuring narrow LSPR bands, regardless of the aspect ratio (FWHM = 0.250 eV at 600 nm; FWHM = 0.177 eV at 800 nm; FWHM = 0.165 eV at 1000 nm; FWHM = 0.187 eV at 1250 nm). AuNR dimensions could be readily varied between 40 and 103 nm in length and between 15 and 25 nm in width, with an average volume of $(18 \pm 2) \times 10^3$ nm^3 (**Figure 6E–H**, **Figure S24**, **Tables S6 and S7**). The dispersity in aspect ratio, as determined from LSPR bands, consistently ranged between 7% and 11%, *i.e.* within the state-of-the-art values of typical syntheses of short rods (**Figure 6B, Figure S24, Tables S8** and **S9**). Although selected approaches for the preparation of AuNRs with LSPR wavelengths either above 1150 nm[29,46,47] or below 650 nm[48] have been reported, the dispersity and/or shape purity of the products was generally poor. In our case, when the $[HCl]/[HAuCl_4]$ ratio was increased up to 240 and temperature decreased down to 16 °C, the growth kinetics was slowed down to such an extent that the synthesis of AuNRs in the 1200–1300 nm range was readily achieved (an interesting advantage of using *n*-decanol as co-surfactant is the resulting decrease in the Kraft temperature of CTAB. The *n*-decanol/CTAB systems remains stable at temperatures above 16 °C, $[HAuCl_4]/[AgNO_3] = 3.3$; **Figure 6A,F**). Above 1300 nm, the polydispersity in aspect ratio starts to increase and further addition of HCl does not lead to further increasing the aspect ratio (Figure S25). This is the standard limit in the synthesis of high-quality single crystal gold nanorods.[46] Furthermore, the use of reducing agents other than ascorbic acid, for instance hydroquinone, allowed us to obtain low aspect ratio AuNRs, with LSPRs close to 600 nm (**Figure 6A,C**). Due to the different nature and redox potential of hydroquinone

(lower than that of ascorbic acid), we found that the optimal [$HAuCl_4$]/[$AgNO_3$] ratio was also significantly different (*ca.* 10) and HCl was not even required.

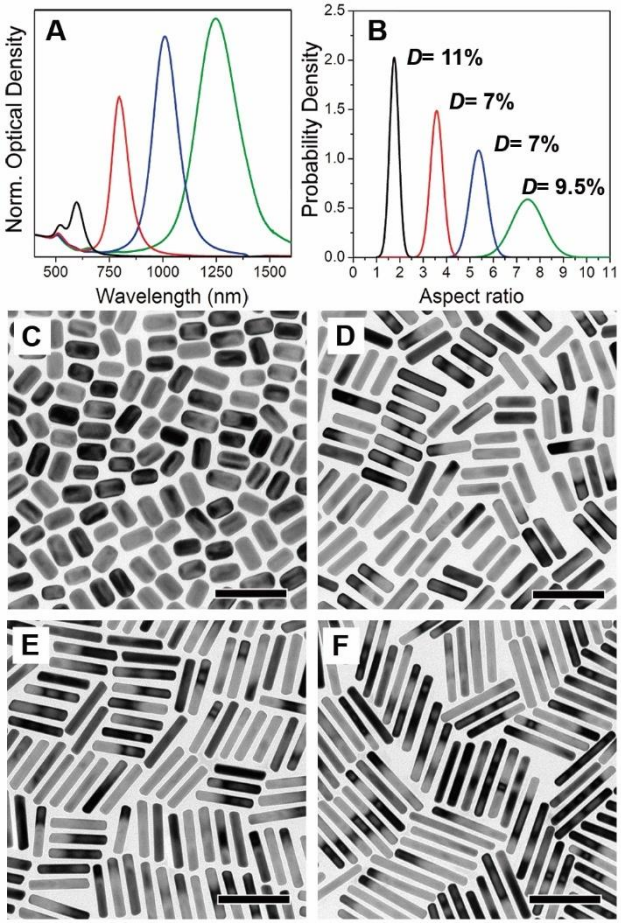

Figure 6. Preparation of AuNRs with tunable, narrow LSPR bands by seeding the growth with small anisotropic seeds. (A) Normalized optical density spectra for selected syntheses. (B) Corresponding *D* derived from optical fits. (C,D) representative TEM images of AuNRs from the colloidal samples in (A,B). Scale bars: 100 nm.

Another important advantage of the synthesis of colloidal AuNRs seeded with small AuNRs is related to control over the absorption and scattering cross-sections. It has been well stablished that absorption dominates in the case of small AuNRs, whilst scattering may become dominant at larger sizes.[28,49] Herein, by simply adjusting the amount of small AuNRs

added to the growth solution, we were able to fine-tune the size of the final AuNRs. A proof-of-concept test was carried out by growing AuNRs with a five-fold increased volume (standard AuNR volume: (15–25) × 10^3 nm^3, **Figure 7C–F**). The LSPR wavelength was mainly governed by pH, while size uniformity was ensured by a suitable [$HAuCl_4$]/[$AgNO_3$] ratio. For a volume of (74 ± 4) × 10^3 nm^3, the LSPR wavelength could be tuned from 600 to 1110 nm, while length and width varied from 60 to 140 nm and 20 to 40 nm, respectively (**Figure 7A–D**, **Figure S26**, **Tables S8 and S9**). When the seed concentration was increased, colloidal AuNRs were obtained with an average volume of (4.3 ± 0.7) × 10^3 nm^3 and LSPR bands ranging from 600 to 1050 nm. The corresponding dimensions varied between 30 and 55 nm in length and between 8 and 13 nm in width (**Figure 7E–H**, **Figure S26**). It should be noted that, in conventional methods a variation in the number of seeds requires re-optimization of the synthesis and modification of multiple parameters, whereas hardly any optimization was required to obtain high-quality AuNRs with the present method (*D* values of 9–13% and 12–15% for AuNRs with large and small volumes, respectively; see **Figure S26**, **Tables S8** and **S9**).

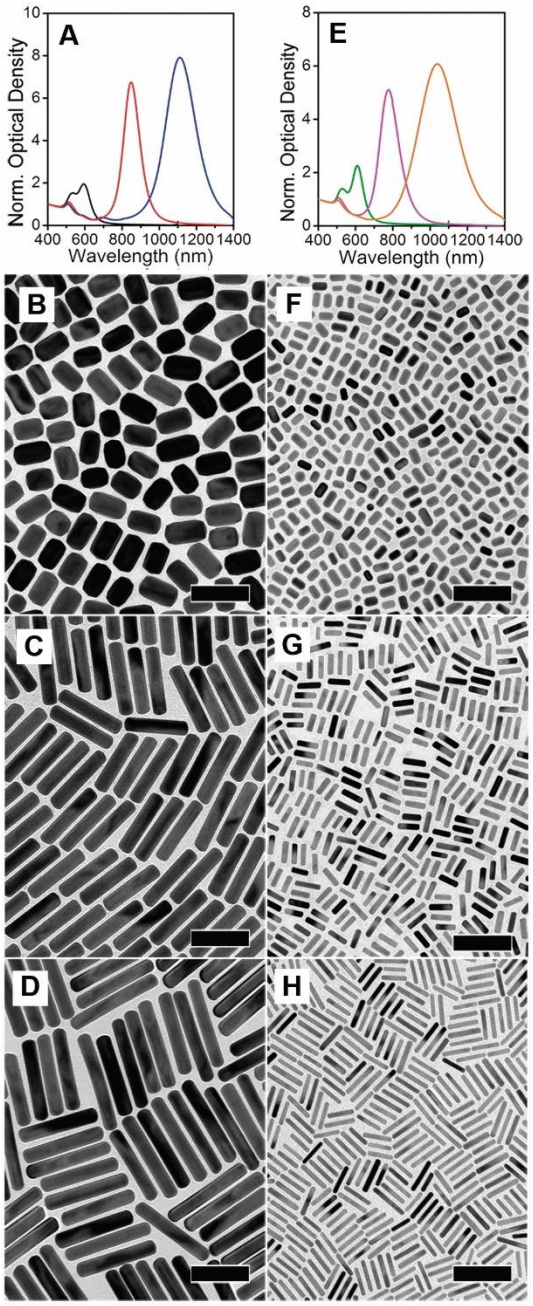

Figure 7. Tuning AuNR size. (A) Normalized optical density and (B–D) TEM images of AuNRs displaying an average volume of (74 ± 4) × 10^3 nm^3 and LSPR bands located at 600 (black, B), 850 (red, C), and 1110 (blue, D) nm. (E) Normalized optical density and (F–H) TEM images of AuNRs displaying an average volume of (4.3 ± 0.7) × 10^3 nm^3 and LSPR bands located at 610 (green, F), 775 (magenta, G), and 1040 (orange, H) nm. Scale bars: 100 nm.

Optimization of a synthetic procedure requires modification of multiple parameters, which in practice implies that only a narrow range of conditions are allowed.[19–21,29] Furthermore, the symmetry breaking event is highly sensitive to small variations in the concentrations of various reagents during 1–2 nm seed preparation (*e.g.* stirring speed during $NaBH_4$ addition or its decomposition).[21,25,26] Therefore, the reproducibility and reliability of commonly employed methods becomes elusive. We found that the superior control obtained through the use of small anisotropic nanocrystals as seeds and the addition of *n*-decanol, significantly improves the reproducibility of the method. To illustrate this idea, we carried out a series of AuNR syntheses. Furthermore, we used water provided by colleagues from different laboratories worldwide and CTAB with different qualities to introduce plausible sources of non-reproducibility (water and CTAB have been claimed as common sources of reproducibility).[21] Water samples were thus obtained from labs in Australia, Brazil, China, USA, Germany, India, and Italy (see details in the Supporting Information). Our results show that high-quality AuNR colloids were systematically obtained, thereby confirming the high reproducibility of the present method. A high level of control over the LSPR, aspect ratio dispersity and NR size was demonstrated (**Figure S27-S31**, **Table S10**), even though no further optimization was performed (see the re-optimization route in the Supplementary Information, **Figure S32**, **Tables S11-S13**).

The robustness of this method lies on the disconnection of the symmetry breaking event and the growth process. While the range of reagent concentrations and temperatures is still very narrow for the synthesis of small anisotropic seeds (see **Figure 2**), the homogeneity of the growth process is much less sensitive to variations in the experimental conditions (**Figures 4–7**). Hence, once small AuNRs have been obtained in high yield, after symmetry breaking under optimal experimental conditions, it is very unlikely that low quality AuNRs will be

obtained or that control over their aspect ratio and dimensions will be lost during the growth step.

CONCLUSIONS

In summary, we demonstrate that the reproducibility, tunability and even quality of colloidal gold nanorods can be largely improved by dealing separately with symmetry breaking and seeded growth. Symmetry breaking is first optimized to produce uniform small AuNRs, using *n*-decanol to enhance the face-selective capping properties of CTAB. In a second step, these anisotropic nanocrystals are employed as universal, anisotropic seeds for the growth of high-quality AuNR colloids with tailored aspect ratios and/or dimensions. This approach yields AuNRs with LSPRs that can be broadly tuned, with high simplicity, from 600 up to 1250 nm. Additionally, low aspect ratio dispersity is obtained, regardless of the aspect ratio and size of the prepared colloidal AuNRs. We also demonstrate that disconnecting symmetry breaking from growth leads to improved reproducibility and reliability of the synthesis, which has traditionally been one of the main pending issues toward large scale AuNR synthesis. The uncertainty associated with the symmetry breaking process is significantly reduced in comparison with standard methods, where each AuNR synthesis requires manipulation of both symmetry breaking and growth, regardless of the final aspect ratio and size. Finally, whereas most syntheses are based on one-pot approaches, where the experimental conditions for symmetry breaking and growth are the same, we show that both stages require different experimental conditions and independent optimization leads to high-quality AuNRs.

METHODS

Chemicals. All the starting materials were obtained from Sigma Aldrich and used without further purification: hexadecyltrimethylammonium bromide (CTAB for molecular biology ≥99%, batch code BCBBT066; CTAB 96%, batch code: BCBB0800; CTAB BioXtra ≥99% batch code: BCBS1424V), hexadecyltrimethylammonium chloride (CTAC, 25% w/w aqueous solution), 1-decanol (*n*-decanol, 98%), hydrogen tetrachloroaurate trihydrate ($HAuCl_4 \cdot 3H_2O$, ≥99.9%), silver nitrate ($AgNO_3$, ≥99.0%), hydroquinone (≥99.0%), sodium tetrachloropalladate (Nd_2PdCl_4, 98%), L-ascorbic acid (≥99%), and sodium borohydride ($NaBH_4$, 99%) were purchased from Aldrich. MilliQ grade water (resistivity 18.2 MΩ cm at 25 °C) was used in all experiments.

***n*-decanol/CTAB Solution.** The growth solution was prepared by dissolving 9.111 g of CTAB (50 mM) and 1.068 g (13.5 mM for 1-2 nm and 21 × 7.5 nm seeds) or 870.5 mg (11 mM for AuNR synthesis) of *n*-decanol in 500 mL of warm water (stirring at ~60 °C for 1 h or 30 °C overnight) in a 500 mL Erlenmeyer flask. Importantly, CTAB and *n*-decanol were weighted directly in the Erlenmeyer flask. Once *n*-decanol is incorporated in CTAB micelles, the solution is stable while the temperature is kept above 16°C.

Synthesis of 1–2 nm Gold Seeds. A 0.05 M $HAuCl_4$ solution (200 μL) and 100 μL of a 0.1 M ascorbic acid solution were added to 20 mL of a 50 mM CTAB and 13.5 mM *n*-decanol solution in a 50 mL glass beaker at 25–27 °C. A colorless solution was obtained. After 1–2 min, 800 μL of a freshly prepared 0.02 M $NaBH_4$ solution was injected under vigorous stirring (1000 rpm using a PTFE plain magnetic stirring bar: 30 × 6 mm) at 25–27 °C giving rise to a brownish-yellow solution (Movie S1). Excess borohydride was consumed by ageing the seed solution for at least 60 min at 25–27 °C prior to use. In the case of standard AuNRs,

1-2 nm gold seeds were prepared using a 100 mM CTAB solution instead of 50 mM CTAB and 13.5 mM *n*-decanol solution.

Synthesis of Small Anisotropic Seeds (21 nm in length and 7.5 nm in width). In a typical synthesis, 2400 µL of 0.01 M $AgNO_3$, 21 mL of 1 M HCl, 3000 µL of 0.05 M $HAuCl_4$, and 3900 µL of 0.1 M ascorbic acid were added to 300 mL of a 50 mM CTAB and 11 mM *n*-decanol solution at exactly 25 °C. Then, 18 mL of the seed solution was added under stirring. The mixture was left undisturbed at exactly 25 °C for at least 4 h. The solution changed from colorless to grey and finally dark brownish gray. The longitudinal LSPR of the small anisotropic nanocrystals at this point should be located at 725–730 nm. The obtained small anisotropic seeds were centrifuged at 14000–15000 rpm for 45–60 min in 2 mL tubes. The precipitate was re-dispersed with 4 mL of a 10 mM CTAB solution. The concentrated gold nanorod colloid was centrifuged twice under the same conditions. Finally, the final Au^0 concentration was fixed to 4.65 mM (Abs_{400nm}: 10, optical path: 1 cm).

Synthesis of Small Anisotropic Seeds in the absence of *n*-decanol. In a typical synthesis, 120 µL of 0.01 M $AgNO_3$, 20 µL of 1 M HCl, 100 µL of 0.05 M $HAuCl_4$, and 80 µL of 0.1 M ascorbic acid were added to 10 mL of a 100 mM CTAB at exactly 28 °C. Then, 12 µL of the seed solution (prepared following the same protocol described for the 1-2 nm gold cluster synthesis but using 100 mM CTAB instead of 50 mM CTAB and 13.5 mM *n*-decanol solution) was added under stirring. The mixture was left undisturbed at 28 °C for at least 4 h. The solution changed from colorless to grey and finally dark brownish orange. The longitudinal LSPR of the small anisotropic nanocrystals at this point should be located at 800 nm. The obtained small anisotropic seeds were centrifuged at 14000–15000 rpm for 45–60 min in 2 mL tubes. The precipitate was re-dispersed with 4 mL of a 10 mM CTAB solution. The concentrated gold nanorod colloid was centrifuged twice under the same conditions.

Synthesis of Small Gold@Palladium Anisotropic Seeds. A protocol previously described was followed.[18] Briefly, 1.2 mL of a small anisotropic nanocrystals suspension (Au conc. = 4.65 mM, Abs_{400nm}: 10, optical path: 1 cm) was centrifuged at 14000–15000 rpm for 45–60 min using 2 mL tubes. The precipitate was re-dispersed in 2 mL of a 50 mM CTAC solution. This step was repeated twice and the nanoparticles were finally re-dispersed in 20 mL of 50 mM CTAC. Then, 250 µL of 5 mM Na_2PdCl_4 and 250 µL of 0.1 M ascorbic acid were added under mild stirring. The mixture was left undisturbed at 40 °C for 12 h. The final colloids were removed from the growth solution by centrifugation at 14000 rpm for 45–60 min and re-dispersed in 1-2 mL of 2 mM CTAC.

Synthesis of Gold Nanorods with Tunable LSPR Bands and Dimensions. In a typical synthesis, a certain amount of a 0.01 M $AgNO_3$ solution (**Table S11–S13**), 100 µL of 0.05 M $HAuCl_4$, 80 µL of a 0.1 M ascorbic acid solution (LSPRs between 660 nm and 1270 nm) or 500 µL of a 0.1 M hydroquinone solution (LSPRs close to 600 nm) were added under stirring to 10 mL of a 50 mM CTAB and 11 mM *n*-decanol solution at a given temperature (**Table S11-S13**). Then, a certain volume of 1 M HCl was added (**Table S11-S13**). The size of the AuNRs was controlled by the addition of: 10 µL (V_f: 74×10^3 nm^3), 50 µL (V_f: 16×10^3 nm^3), or 250 µL (V_f: ca. 3000×10^3 nm^3) of the small anisotropic seed suspension.

Synthesis of Gold Nanorods Using the Standard Method. A two-steps standard method for the synthesis of AuNRs was used with minor modifications.[11] In a typical synthesis, 120 µL of a 0.01 M $AgNO_3$, 100 µL of 0.05 M $HAuCl_4$, 200 µL of 1M HCl and 80 µL of 0.1 M ascorbic acid solution were added under stirring to 10 mL of a 100 mM CTAB solution at a 28°C. Then, the growth was initiated by adding 12 µL of seed solution. The mixture was left undisturbed until the growth was completed (4 hours).

Characterization. *Transmission Electron Microscopy (TEM):* Low magnification TEM images were obtained on a JEOL JEM-1400PLUS transmission electron microscope operating at an acceleration voltage of 120 kV. Carbon-coated 400 square-mesh copper grids were used. *Small Gold@Palladium Anisotropic Seeds:* HAADF-STEM images were acquired using a FEI Tecnai Osiris electron microscope operated at 200 kV. Acquisition of the electron tomography tilt series was performed in HAADF-STEM mode and a Fischione model 2020 single-tilt tomography holder was used. The tilt series were acquired over an angular range of ±74° with a tilt increment of 2°. The reconstruction was performed using the Simultaneous Iterative Reconstruction Technique (SIRT) implemented in the ASTRA toolbox, where 100 iterations were used. *Gold cluster characterization:* HAADF-STEM images were acquired using an aberration corrected cubed FEI-Titan electron microscope operated at 300kV. *TEM Grid Preparation*: 5 mL of the mixture (Au(0) concentration of 0.5 mM and surfactant concentration of 50 mM) was centrifuged and redispersed in 1 mL of a 1 mM CTAB solution; then, the NRs were centrifuged again (same parameters) and redispersed with 200 μL of water (Au(0) concentration of 25 mM and CTAB concentrations ranging 0.1–0.2 mM). Finally, one drop (3 μL) was allowed to dry slowly on a carbon-coated 400 square-mesh copper grid (placed on Parafilm). *UV-vis-NIR Spectroscopy*: Extinction spectra were recorded using Agilent 8453 UV-vis diode-array and Cary 5000 UV-Vis-NIR spectrophotometers. All experiments were carried out at 298 K using quartz cuvettes with an optical path length of either 2 mm or 1 cm. *^{1}H NMR Spectroscopy:* All the NMR measurements were carried out at 298 K in a Bruker AVIII 700 MHz spectrometer (16.4 T). The proton spectra were recorded by averaging 32 scans, with a digital resolution of 0.30 Hz. The signal assignment of the surfactant was established by conventional NMR methods (correlation spectroscopy, total correlation spectroscopy). *Diffusion-ordered NMR spectroscopy (DOSY):* A stimulated echo sequence incorporating bipolar gradients

(BPPLED) with a longitudinal eddy current delay of 5 ms was used for acquiring DOSY spectra. The duration of the magnetic field pulse gradients and the diffusion times were optimized for each sample to observe the complete signal decay with the maximum gradient strength. Gradient strengths of 2.0-2.5 ms were incremented in 32 steps ranging between 2% and 95% of the total gradient using a linear ramp. An exponential window function with 1 Hz line broadening was applied before Fourier transformation.[34]

***n*-Decanol/CTAB Micelles on Gold:** With the aim of understanding the role of *n*-decanol on the structure of CTA^+ aggregates and its effect on the nanorod growth, we performed Molecular Dynamics simulations of a CTA^+ bilayer deposited on top of a gold surface. The co-surfactant *n*-decanol was inserted at random positions of the CTAB bilayer. Both amphiphilic molecules were modeled with the GROMOS53-a6 force fields as the starting point.[50] However, the partial charges of CTA^+ and *n*-decanol were assigned values obtained from the *ab-initio* calculations described in our previous works.[51] Bromide, which acts as the counter-ion of CTA^+, was described as a Lennard-Jones (LJ) potential with a negative charge at its center.[52] The atoms forming the surface were described with the model developed by Heinz *et al.*[52] The system was then solvated with SPC water, adding gold ions in the form of $AuCl_2^-$ and hydronium (H_3O^+) to neutralize the system. $AuCl_2^-$ was described with the same model used by Mena *et al.*,[53] whereas hydronium was modelled as an LJ center with charges in tetrahedral symmetry. Three positive charges +0.529 were placed one in each hydrogen, and a negative charge (-0.587) at the oxygen atom. The hydronium charges were obtained with the Automated Topology Builder. The O–H bond length was set to 0.0983 nm, and the strength in the bond was constant at 9 831 400 kJ mol^{-1} nm^{-2}.[51] Simulations were performed at varying CTA^+/ *n*-decanol ratios from 0 to 0.5 for four different gold surfaces, namely,{100},{110},{111}, and {250}. Further details about the simulated systems are provided in **Table S1** of the Supporting Information.

Simulations were performed with the GROMACS package in the NPT ensemble at 1 bar and 298 K. The temperature was controlled with a velocity-rescale thermostat and the pressure with a Berdensen barostat.[54,55] Equations of motion were integrated with a time step of 0.003 ps. The relaxation times of the barostat and thermostat were set at 2 ps. The LJ potential as well as the real part of electrostatic interactions were truncated at 1.2 nm. The Particle–Particle mesh technique was used to deal with electrostatic interactions.[56] Initial pre-assembled configurations of the CTA^+Br^-/ *n*-decanol bilayers were created using Packmol.[36] The gold surface and the bilayer were placed perpendicular to the *z*-axis. Gold surfaces were placed at the bottom and top of the simulation box. Periodic boundary conditions were applied in the three dimensions of space but leaving 10 nm of vacuum between the two gold surfaces to avoid interactions between neighboring images of the cell. To correct overlaps in the initial configuration, a steep descent minimization was performed until the maximum force converged at 1000 kJ mol^{-1} nm^{-1}. Simulations were extended over rather long times of about 45–425 ns, since the diffusion of gold ions through the CTA^+ aggregate to the gold surface is a rather slow process (see **Table S1** in Supporting Information). Previous simulations of the assembly of CTAB in the presence of the *n*-decanol showed that the co-surfactant stabilizes the bilayers over a rather wide *n*-decanol concentration range. Here, we analyzed the structure of the aggregates as a function of the *n*-decanol concentration when deposited on top of the gold surfaces by plotting 2D density maps. The orientational order of CTA^+ molecules was quantified by evaluating the parameter $S_z = 1/2 <3 \cos \theta^2 - 1>$, where θ is the angle formed by the head-to-tail vector of each surfactant molecule with the *z*-axis. The availability of gold ions on the gold surfaces was estimated by measuring the distribution of ions as a function of the distance to the surface $P(z)$ along the *z*-axis (see Figure S3 in the Supporting Information) and calculating the average distribution function within a distance of 1 nm from the surface.

Dispersity Measurements and Calculations. The size and aspect ratio distributions of the AuNRs were obtained from analysis of the TEM images, following the protocol previously reported by Hubert *et al.*[57] The Image J software with the algorithm "Measure_ROI.class" was employed to obtain the length and diameter of the gold nanorods from the TEM images. About 50–300 nanoparticles per sample were measured.

Simulating the optical response of Au nanorods ensemble and fitting to the optical spectra. The simulation of the optical density of an ensemble of gold nanorods, or any other nanoparticles, implies a large number of calculations (equation 1). This fact requires that the selected method for calculating the optical extinction of the particles cannot be computationally expensive due to the long time it would demand. In this work we have used an approach to calculate the ensemble extinction cross section ($\langle\sigma_{ext}\rangle$, equation 2) which is based on an extension of the electrostatic approximation.[43] This extension of the electrostatic approximation includes retardation effects for arbitrary geometries like cylinders, spheroids or hemispherically capped cylinders, allowing a rapid calculation of their cross sections without the necessity of expensive numerical methods. The hemispherically capped cylinder geometry is used directly due to its similarity with the synthesized colloidal nanorods. Also the medium refractive index does not need to be corrected, so in this case, a refractive index slightly lower than the CTAB index (*i.e.* 1.435)[58] of 1.400 is used due to the presence of water molecules around the surface of the particles. The broadening and position of the optical spectra depends on the aspect ratio dispersity to a great extent and less to the volume distribution of the particles. Because of this, we consider nanorods with constant volume (V, with equivalent sphere radius of R_v) and a normal distribution of aspect ratios ($n(\rho)$), where the mean value (ρ_n) and standard deviation (σ_n) are the fitting parameters.

$$\langle OD \rangle = log(e) CL \langle \sigma_{ext} \rangle \quad (1)$$

$$\langle \sigma_{ext} \rangle = \int_{\rho_{min}}^{\rho_{max}} n\,(\rho) \sigma_{ext}(V, \rho) d\rho = \sum_{i=1}^{M} u_i\, n(\rho_i) \sigma_{ext}(V, \rho_i) \quad (2)$$

$$\sigma_{ext}(V, \rho_i) = \frac{2 \cdot \sigma_{ext,trans}(V, \rho_i) + \sigma_{ext,long}(V, \rho_i)}{3} \quad (3)$$

The calculation of the ensemble optical density and the fitting procedure to the optical measurements can be revised elsewhere (see Supporting Information for more detailed discussion).[6,44,59] To take in account unpolarized light and random orientation of the nanoparticles, the longitudinal ($\sigma_{ext,long}$) and transversal ($\sigma_{ext,trans}$) responses are averaged and the fitting results compared to the T-matrix method (equation 3, see Supporting Information).

ASSOCIATED CONTENT

The following files are available free of charge on ACS Publications website:

Information about the: symmetry breaking process, computational simulation of the n-decanol/CTAB system, the role of small-AuNR size on the synthesis of high-quality AuNRs, the effect of *n*-decanol/CTAB ratio on the growth process, comparison of the use of small AuNRs and standard Au nanocrystal seeds in the growth of AuNRs at increasing [HCl]/[$HAuCl_4$] ratios, the dependence of the optimal [$HAuCl_4$]/[$AgNO_3$] ratio with the temperature, the preparation of AuNRs with tunable, narrow LSPR bands by seeding the growth with small AuNRs, tuning the AuNR size, the growth of AuNRs using water from different countries, protocol for small-AuNR synthesis optimization and the simulation of the optical response of AuNR ensembles and optical spectrum fitting (pdf).

Movie S1 shows the synthesis of 1-2 nm gold seeds.

AUTHOR INFORMATION

*Address correspondence to ggrubio@ucm.es, aguerrero@quim.ucm.es and llizmarzan@cicbiomagune.es

ACKNOWLEDGMENT

This work has been funded by the Spanish MINECO (FIS2017-89361-C3-2-P and MAT2017-86659-R), the Madrid Regional Government (P2018/NMT-4389) and the Complutense University of Madrid (PR75/18-21616). Funding is acknowledged from the European Commission (grant EUSMI 731019). G.G.-R. acknowledges receipt of FPI Fellowship from the Spanish MINECO. E.B. and T.A. acknowledge postdoctoral grants from the Research Foundation Flanders (FWO). The authors are indebted to Profs. Justing Gooding, Watson Loh, Nicholas Kotov, Deqing Zhang, Mihaela Delcea, Maurizio Prato and Krishna Ganesh, for providing milli-Q water samples.

REFERENCES

(1) Dreaden, E. C.; Alkilany, A. M.; Huang, X.; Murphy, C. J.; El-Sayed, M. A. The Golden Age: Gold Nanoparticles for Biomedicine. *Chem. Soc. Rev.* **2012**, *41*, 2740–2779.

(2) Bej, A.; Ghosh, K.; Sarkar, A.; Knight, D. W. Palladium Nanoparticles in the Catalysis of Coupling Reactions. *RSC Adv.* **2016**, *6*, 11446–11453.

(3) Deng, Y.; Xue, H.; Lu, S.; Song, Y.; Cao, X.; Wang, L.; Wang, H.; Zhao, Y.; Gu, H. Trimetallic Au@PtPd Mesoporous Nanorods as Efficient Electrocatalysts for the Oxygen Reduction Reaction. *ACS Appl. Energy Mater.* **2018**, *1*, 4891–4898.

(4) Bodelón, G.; Montes-García, V.; López-Puente, V.; Hill, E. H.; Hamon, C.; Sanz-Ortiz, M. N.; Rodal-Cedeira, S.; Costas, C.; Celiksoy, S.; Pérez-Juste, I.; Liz-Marzán, L. M. Detection and Imaging of Quorum Sensing in Pseudomonas Aeruginosa Biofilm Communities by Surface-Enhanced Resonance Raman Scattering. *Nat. Mater.* **2016**, *15*, 1203–1211.

(5) Xia, Y.; Xiong, Y.; Lim, B.; Skrabalak, S. E. Shape-Controlled Synthesis of Metal Nanocrystals: Simple Chemistry Meets Complex Physics? *Angew. Chem. Int. Ed.* **2009**, *48*, 60–103.

(6) González-Rubio, G.; Díaz-Núñez, P.; Rivera, A.; Prada, A.; Tardajos, G.; González-Izquierdo, J.; Bañares, L.; Llombart, P.; Macdowell, L. G.; Palafox, M. A.; Liz-Marzán, L. M.; Peña-Rodríguez, O. Guerrero-Martínez, A. Femtosecond Laser

Reshaping Yields Gold Nanorods with Ultranarrow Surface Plasmon Resonances. *Science* **2017**, *358*, 640–644.
(7) Jana, N. R.; Gearheart, L.; Murphy, C. J. Seed-Mediated Growth Approach for Shape-Controlled Synthesis of Spheroidal and Rod-like Gold Nanoparticles Using a Surfactant Template. *Adv. Mater.* **2001**, *13*, 1389–1393.
(8) Jana, N. R.; Gearheart, L.; Murphy, C. J. Wet Chemical Synthesis of High Aspect Ratio Cylindrical Gold Nanorods. *J. Phys. Chem. B* **2001**, *105*, 4065–4067.
(9) Xia, Y.; Gilroy, K. D.; Peng, H.-C.; Xia, X. Seed-Mediated Growth of Colloidal Metal Nanocrystals. *Angew. Chem. Int. Ed.* **2017**, *56*, 60–95.
(10) Hanske, C.; González-Rubio, G.; Hamon, C.; Formentín, P.; Modin, E.; Chuvilin, A.; Guerrero-Martínez, A.; Marsal, L. F.; Liz-Marzán, L. M. Large-Scale Plasmonic Pyramidal Supercrystals *via* Templated Self-Assembly of Monodisperse Gold Nanospheres. *J. Phys. Chem. C* **2017**, *121*, 10899–10906.
(11) Nikoobakht, B.; El-Sayed, M. A. Preparation and Growth Mechanism of Gold Nanorods (NRs) Using Seed-Mediated Growth Method. *Chem. Mater.* **2003**, *15*, 1957–1962.
(12) Scarabelli, L.; Coronado-Puchau, M.; Giner-Casares, J. J.; Langer, J.; Liz-Marzán, L. M. Monodisperse Gold Nanotriangles: Size Control, Large-Scale Self-Assembly, and Performance in Surface-Enhanced Raman Scattering. *ACS Nano* **2014**, *8*, 5833–5842.
(13) Tong, W.; Walsh, M. J.; Mulvaney, P.; Etheridge, J.; Funston, A. M. Control of Symmetry Breaking Size and Aspect Ratio in Gold Nanorods: Underlying Role of Silver Nitrate. *J. Phys. Chem. C* **2017**, *121*, 3549–3559.
(14) Walsh, M. J.; Tong, W.; Katz-Boon, H.; Mulvaney, P.; Etheridge, J.; Funston, A. M. A Mechanism for Symmetry Breaking and Shape Control in Single-Crystal Gold Nanorods. *Acc. Chem. Res.* **2017**, *50*, 2925–2935.
(15) Walsh, M. J.; Barrow, S. J.; Tong, W.; Funston, A. M.; Etheridge, J. Symmetry Breaking and Silver in Gold Nanorod Growth. *ACS Nano* **2015**, *9*, 715–724.
(16) Ye, X.; Jin, L.; Caglayan, H.; Chen, J.; Xing, G.; Zheng, C.; Doan-Nguyen, V.; Kang, Y.; Engheta, N.; Kagan, C. R.; Murray, C. B. Improved Size-Tunable Synthesis of Monodisperse Gold Nanorods through the Use of Aromatic Additives. *ACS Nano* **2012**, *6*, 2804–2817.
(17) Ye, X.; Zheng, C.; Chen, J.; Gao, Y.; Murray, C. B. Using Binary Surfactant Mixtures To Simultaneously Improve the Dimensional Tunability and Monodispersity in the Seeded Growth of Gold Nanorods. *Nano Lett.* **2013**, *13*, 765–771.
(18) Scarabelli, L.; Grzelczak, M.; Liz-Marzán, L. M. Tuning Gold Nanorod Synthesis through Prereduction with Salicylic Acid. *Chem. Mater.* **2013**, *25*, 4232–4238.
(19) Gao, J.; Bender, C. M.; Murphy, C. J. Dependence of the Gold Nanorod Aspect Ratio on the Nature of the Directing Surfactant in Aqueous Solution. *Langmuir* **2003**, *19*, 9065–9070.
(20) Rodríguez-Fernández, J.; Pérez-Juste, J.; Mulvaney, P.; Liz-Marzán, L. M. Spatially-Directed Oxidation of Gold Nanoparticles by Au(III)−CTAB Complexes. *J. Phys. Chem. B* **2005**, *109*, 14257–14261.
(21) Scarabelli, L.; Sánchez-Iglesias, A.; Pérez-Juste, J.; Liz-Marzán, L. M. A "Tips and Tricks" Practical Guide to the Synthesis of Gold Nanorods. *J. Phys. Chem. Lett.* **2015**, *6*, 4270–4279.
(22) Sánchez-Iglesias, A.; Winckelmans, N.; Altantzis, T.; Bals, S.; Grzelczak, M.; Liz-Marzán, L. M. High-Yield Seeded Growth of Monodisperse Pentatwinned Gold Nanoparticles through Thermally Induced Seed Twinning. *J. Am. Chem. Soc.* **2017**, *139*, 107–110.

(23) González-Rubio, G.; Oliveira, T. M. de; Altantzis, T.; Porta, A. L.; Guerrero-Martínez, A.; Bals, S.; Scarabelli, L.; M. Liz-Marzán, L. Disentangling the Effect of Seed Size and Crystal Habit on Gold Nanoparticle Seeded Growth. *Chem. Commun.* **2017**, *53*, 11360–11363.
(24) Gole, A.; Murphy, C. J. Seed-Mediated Synthesis of Gold Nanorods: Role of the Size and Nature of the Seed. *Chem. Mater.* **2004**, *16*, 3633–3640.
(25) Park, K.; Hsiao, M.-S.; Koerner, H.; Jawaid, A.; Che, J.; Vaia, R. A. Optimizing Seed Aging for Single Crystal Gold Nanorod Growth: The Critical Role of Gold Nanocluster Crystal Structure. *J. Phys. Chem. C* **2016**, *120*, 28235–28245.
(26) Burrows, N. D.; Harvey, S.; Idesis, F. A.; Murphy, C. J. Understanding the Seed-Mediated Growth of Gold Nanorods Through a Fractional Factorial Design of Experiments. *Langmuir* **2017**, *33*, 1891–1907.
(27) Ali, M. R. K.; Snyder, B.; El-Sayed, M. A. Synthesis and Optical Properties of Small Au Nanorods Using a Seedless Growth Technique. *Langmuir* **2012**, *28*, 9807–9815.
(28) Jia, H.; Fang, C.; Zhu, X.-M.; Ruan, Q.; Wang, Y.-X. J.; Wang, J. Synthesis of Absorption-Dominant Small Gold Nanorods and Their Plasmonic Properties. *Langmuir* **2015**, *31*, 7418–7426.
(29) Chang, H.-H.; Murphy, C. J. Mini Gold Nanorods with Tunable Plasmonic Peaks beyond 1000 nm. *Chem. Mater.* **2018**, *30*, 1427–1435.
(30) Karayil, J.;Kumar, S.;Hassan, PA, Talmon, Y.; Sreejith, L. Microstructural Transition of Aqueous CTAB Micelles in the Presence of Long Chain Alcohols. *RSC Adv*. **2015**, *5*, 12434-12441
(31) Liu, M.; Guyot-Sionnest, P. Mechanism of Silver(I)-Assisted Growth of Gold Nanorods and Bipyramids. *J. Phys. Chem. B* **2005**, *109*, 22192–22200.
(32) Almora-Barrios, N.; Novell-Leruth, G.; Whiting, P.; Liz-Marzán, L. M.; López, N. Theoretical Description of the Role of Halides, Silver, and Surfactants on the Structure of Gold Nanorods. *Nano Lett.* **2014**, *14*, 871–875.
(33) Meena, S. K.; Celiksoy, S.; Schäfer, P.; Henkel, A.; Sönnichsen, C.; Sulpizi, M. The Role of Halide Ions in the Anisotropic Growth of Gold Nanoparticles: A Microscopic, Atomistic Perspective. *Phys. Chem. Chem. Phys.* **2016**, *18*, 13246–13254.
(34) Guerrero-Martínez, A; Montoro, T.; Viñas, M. H.; González-Gaitano, G.; Tardajos, G. Study of the Interaction Between a Nonylphenylether and β-Cyclodextrin: Declouding Nonionic Surfactant Solutions by Complexation. *J. Phys. Chem. B* **2007**, *111*, 1368-1376.
(35) Pronk, S.; Páll, S.; Schulz, R.; Larsson, P.; Bjelkmar, P.; Apostolov, R.; Shirts, M. R.; Smith, J. C.; Kasson, P. M.; van der Spoel, D.; Hess, B.; Lindahl, E. GROMACS 4.5: A High-Throughput and Highly Parallel Open Source Molecular Simulation Toolkit. *Bioinforma. Oxf. Engl.* **2013**, *29*, 845–854.
(36) Martínez, L.; Andrade, R.; Birgin, E. G.; Martínez, J. M. PACKMOL: A Package for Building Initial Configurations for Molecular Dynamics Simulations. *J. Comput. Chem.* **2009**, *30*, 2157–2164.
(37) Goris, B.; Bals, S.; Van den Broek, W.; Carbó-Argibay, E.; Gómez-Graña, S.; Liz-Marzán, L. M.; Van Tendeloo, G. Atomic-Scale Determination of Surface Facets in Gold Nanorods. *Nat. Mater.* **2012**, *11*, 930–935.
(38) Carbó- Argibay, E.; Rodríguez- González, B.; Gómez- Graña, S.; Guerrero-Martínez, A.; Pastoriza- Santos, I.; Pérez- Juste, J.; Liz- Marzán, L. M. The Crystalline Structure of Gold Nanorods Revisited: Evidence for Higher-Index Lateral Facets. *Angew. Chem. Int. Ed.* **2010**, *49*, 9397–9400.

(39) Khlebtsov, B. N.; Khanadeev, V. A.; Ye, J.; Sukhorukov, G. B.; Khlebtsov, N. G. Overgrowth of Gold Nanorods by Using a Binary Surfactant Mixture. *Langmuir* **2014**, *30*, 1696–1703.
(40) Song, J. H.; Kim, F.; Kim, D.; Yang, P. Crystal Overgrowth on Gold Nanorods: Tuning the Shape, Facet, Aspect Ratio, and Composition of the Nanorods. *Chem. - Eur. J.* **2005**, *11*, 910–916.
(41) Kozek, K. A.; Kozek, K. M.; Wu, W.-C.; Mishra, S. R.; Tracy, J. B. Large-Scale Synthesis of Gold Nanorods through Continuous Secondary Growth. *Chem. Mater.* **2013**, *25*, 4537–4544.
(42) Tong, W.; Katz-Boon, H.; Walsh, M. J.; Weyland, M.; Etheridge, J.; Funston, A. M. The Evolution of Size, Shape, and Surface Morphology of Gold Nanorods. *Chem. Commun.* **2018**, *54*, 3022–3025.
(43) Eustis, S.; El-Sayed, M. A. Determination of the Aspect Ratio Statistical Distribution of Gold Nanorods in Solution from a Theoretical Fit of the Observed Inhomogeneously Broadened Longitudinal Plasmon Resonance Absorption Spectrum. *J. Appl. Phys.* **2006**, *100*, 044324-0443231
(44) Yu, R.; Liz-Marzán, L. M.; Abajo, F. J. G. de. Universal Analytical Modeling of Plasmonic Nanoparticles. *Chem. Soc. Rev.* **2017**, *46*, 6710–6724.
(45) Fan, F.-R.; Liu, D.-Y.; Wu, Y.-F.; Duan, S.; Xie, Z.-X.; Jiang, Z.-Y.; Tian, Z.-Q. Epitaxial Growth of Heterogeneous Metal Nanocrystals: From Gold Nano-Octahedra to Palladium and Silver Nanocubes. *J. Am. Chem. Soc.* **2008**, *130*, 6949–6951.
(46) Vigderman, L.; Zubarev, E. R. High-Yield Synthesis of Gold Nanorods with Longitudinal SPR Peak Greater than 1200 nm Using Hydroquinone as a Reducing Agent. *Chem. Mater.* **2013**, *25*, 1450–1457.
(47) Xu, X.; Zhao, Y.; Xue, X.; Huo, S.; Chen, F.; Zou, G.; Liang, X.-J. Seedless Synthesis of High Aspect Ratio Gold Nanorods with High Yield. *J. Mater. Chem. A* **2014**, *2*, 3528–3535.
(48) Sau, T. K.; Murphy, C. J. Seeded High Yield Synthesis of Short Au Nanorods in Aqueous Solution. *Langmuir* **2004**, *20*, 6414–6420.
(49) Liz-Marzán, L. M. Tailoring Surface Plasmons through the Morphology and Assembly of Metal Nanoparticles. *Langmuir* **2006**, *22*, 32–41.
(50) Oostenbrink, C.; Villa, A.; Mark, A. E.; Gunsteren, W. F. V. A Biomolecular Force Field Based on the Free Enthalpy of Hydration and Solvation: The GROMOS Force-Field Parameter Sets 53A5 and 53A6. *J. Comput. Chem.* **2004**, *25*, 1656–1676.
(51) Malde, A. K.; Zuo, L.; Breeze, M.; Stroet, M.; Poger, D.; Nair, P. C.; Oostenbrink, C.; Mark, A. E. An Automated Force Field Topology Builder (ATB) and Repository: Version 1.0. *J. Chem. Theory Comput.* **2011**, *7*, 4026–4037.
(52) Meena, S. K.; Sulpizi, M. From Gold Nanoseeds to Nanorods: The Microscopic Origin of the Anisotropic Growth. *Angew. Chem. Int. Ed.* **2016**, *55*, 11960–11964.
(53) Meena, S. K.; Sulpizi, M. Understanding the Microscopic Origin of Gold Nanoparticle Anisotropic Growth from Molecular Dynamics Simulations. *Langmuir* **2013**, *29*, 14954–14961.
(54) Berendsen, H. J. C.; Postma, J. P. M.; van Gunsteren, W. F.; DiNola, A.; Haak, J. R. Molecular Dynamics with Coupling to an External Bath. *J. Chem. Phys.* **1984**, *81*, 3684–3690.
(55) Bussi, G.; Donadio, D.; Parrinello, M. Canonical Sampling through Velocity Rescaling. *J. Chem. Phys.* **2007**, *126*, 014101-014107
(56) Darden, T.; York, D.; Pedersen, L. Particle Mesh Ewald: An N·log(N) Method for Ewald Sums in Large Systems. *J. Chem. Phys.* **1993**, *98*, 10089–10092.

(57) Hubert, F.; Testard, F.; Rizza, G.; Spalla, O. Nanorods *versus* Nanospheres: A Bifurcation Mechanism Revealed by Principal Component TEM Analysis. *Langmuir* **2010**, *26*, 6887–6891.
(58) Kekicheff, P.; Spalla, O. Refractive Index of Thin Aqueous Films Confined between Two Hydrophobic Surfaces. *Langmuir* **1994**, *10*, 1584–1591.
(59) Rodríguez-Iglesias, V.; Peña-Rodríguez, O.; Silva-Pereyra, H. G.; Rodríguez-Fernández, L.; Kellermann, G.; Cheang-Wong, J. C.; Crespo-Sosa, A.; Oliver, A. Elongated Gold Nanoparticles Obtained by Ion Implantation in Silica: Characterization and T-Matrix Simulations. *J. Phys. Chem. C* **2010**, *114*, 746–751.